

Research Article

Understanding Fluid Flow during Tectonic Reactivation: An Example from the Flamborough Head Chalk Outcrop (UK)

O. Faÿ-Gomord ¹, C. Allanic,² M. Verbiest,¹ R. Honlet,¹ F. Champenois,¹ M. Bonifacie,³ C. Chaduteau,³ S. Wouters,¹ P. Muchez,¹ E. Lasseur,¹ and R. Swennen ¹

¹Department of Earth and Environmental Sciences, KU Leuven, Celestijnenlaan 200E, 3001 Heverlee, Belgium

²Bureau de Recherches Géologiques et Minières, 3 avenue Claude Guillemin, BP 6009, 45060 Orléans Cedex 2, France

³Institut de Physique du Globe de Paris, Sorbonne Paris Cité, Université Paris Diderot, UMR 7154 CNRS, 75005 Paris, France

Correspondence should be addressed to R. Swennen; rudy.swennen@kuleuven.be

Received 26 September 2017; Revised 11 January 2018; Accepted 6 February 2018; Published 2 May 2018

Academic Editor: Ferenc Molnar

Copyright © 2018 O. Faÿ-Gomord et al. This is an open access article distributed under the Creative Commons Attribution License, which permits unrestricted use, distribution, and reproduction in any medium, provided the original work is properly cited.

Flamborough Head chalks are located at the extremities of E-W and N-S trending fault systems along the Yorkshire coast (UK). Rock deformation is expressed in Selwicks Bay where a normal fault is exposed along with a high density of calcite veins. The fault mineralization is tested using geochemistry. Crosscutting relationships are used to differentiate between three vein generations: a network of parallel veins that are oriented perpendicular to stratigraphy (Group I), hydraulic breccia with typical jigsaw puzzle structure (Group II), and a third generation of calcite veins crosscutting the two previous generations (Group III). Geochemical analyses revealed that all three generations possess the same chemical signature and must reflect successive pulses from the same mineralizing fluid source. Strontium isotope analyses showed that the veins have elevated $^{87}\text{Sr}/^{86}\text{Sr}$ ratios, that is, up to 7.110, while ratios of the chalk matrix equal 7.707. The latter value is in agreement with the signature of Late Cretaceous seawater. Consequently, the source of the fluid is external, reflecting an open system. The radiogenic Sr-isotope ratios, combined with low iron concentration, suggest that fluids migrated through sandy deposits. Fluid inclusion salinities range from 0 to 12 eq. wt% NaCl equiv. with a dominance of very low salinity inclusions, reflecting a meteoric signal. This leads to a model where meteoric fluids stored in an underlying confined sandstone aquifer were remobilized. The wide range of salinities could result from mixing of the meteoric fluid with some more saline fluids present in the rock sequence or from the dissolution of salts in the subsurface. In addition to the understanding of the local paragenetic evolution of the veining in Flamborough Head chalks, this study offers an insight into the way how fluid flows and mineralizes along fault zones.

1. Introduction

Chalk is a fine-grained carbonate rock constituted mostly of coccolith tests and characterized by a wide range of porosities and low permeabilities. Chalk intervals can act as an effective seal for hydrocarbons in the subsurface [1]. Nevertheless, fractured chalks develop a significant structural porosity and an increased permeability [2, 3]. In this respect, the critical role of fault zones in fluid migration has been demonstrated (e.g., [4, 5]) and the importance of including fault damage zones in reservoir models has been proven [6]. Hence, in order to understand and predict the behavior of faults in

subsurface chalk successions, outcrop analogue studies need to be carried out.

The Coniacian-Campanian Chalk of Flamborough Head (UK), located on the southern side of the headland, displays a very complex fracture network, with multiple fracture orientations. The whole chalk section at the study location is intensely fractured by bed-confined normal faults of decimeter to plurimeters length. This fracture network is part of a multiscale polygonal fault system confined to the Coniacian-Campanian chalk deposits [7]. These faults will be referred to as chalk confined fault throughout the article. The outcrops are situated at the intersection of two fault systems:

the E-W trending Howardian–Flamborough Belt and the N-S trending Peak Trough Fault systems. The outcrops have been widely studied and a set of normal fault orientations have been recorded (e.g., [8–10]). Their origin still remains poorly understood and was attributed to a complex multiphase tectonic activity of the North Sea area [11]. Faÿ-Gomord et al. [7] evidenced polygon-shaped fracture networks and argued for a synsedimentary origin of the normal faults confined to Chalk. Polygonal faults display displacements of decimeter-scale and are interpreted as resulting from a single deformation phase in which faults develop to accommodate compactional strain. This study focuses on a basement fault crosscutting the whole stratigraphic succession [12] and cropping out in Selwicks Bay. The fault core is characterized by a 2 to 3 m wide zone of cemented breccia described in great detail by Starmer [13] and Sagi et al. [14]. Over a few dozen meters on both sides of the fault plane, chalk deposits are highly fractured and display a swarm of calcite veins. Sagi et al. [14] suggest that fluid flow in fractured chalk is especially influenced by the protolith, in particular, the presence of interlayered marl horizons. The origin of the fluid precipitating the calcite, however, has not been addressed, and it is therefore unclear whether it originates from the pressure solution of the chalk itself or from an external source.

This paper examines the origin of the fluid and constrains the local paragenetic history based on a petrographical, geochemical, and microthermometric analyses of the veins. Veins can record the physicochemical conditions of the fluids and provide information about the connectivity of fault conduits by inferring fluid migration pathways (e.g., [15, 16]). Because these features are difficult to characterize in the subsurface, the study of outcrop analogues offers an ideal view of the fractures and fault zones and provides information on potential fluid migration in fractured tight chalk. The presence of fault-related calcite-cemented breccia suggests a hydraulic fracturing, associated with overpressured conditions [17]. Fault-related hydraulic breccias are described in chalk, both in Selwicks Bay (UK) [14] and the Omeÿ Quarry (France) [18]. Results discussed in this paper contribute to the understanding of the behavior of fault zones and associated fluid flow patterns in tight chalks.

2. Geological Setting

Flamborough Head is a headland located on the east coast of Yorkshire in the UK. The study area is located in Selwicks Bay (N 54°7′14.07″, W 0°4′52.769″) at the eastern termination of the Howardian–Flamborough Fault Belt. This is a system of deep normal faults formed during the Late Jurassic–Early Cretaceous (Figure 1). The fault network was then reactivated as reverse faults, between Late Cretaceous till Early Cenozoic [19]. The Howardian–Flamborough Fault belt delimits the southeastern part of the Cleveland Basin from the northern part of the Market Weighton Block [19, 20]. A fault network oriented N-S also crosses the study area: the Peak Trough Fault System, which was reactivated as well during the inversion of the Cleveland Basin, during the Cenozoic [21]. The exact timing of the tectonic inversion ranges from the

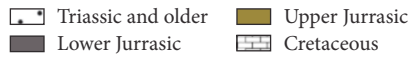
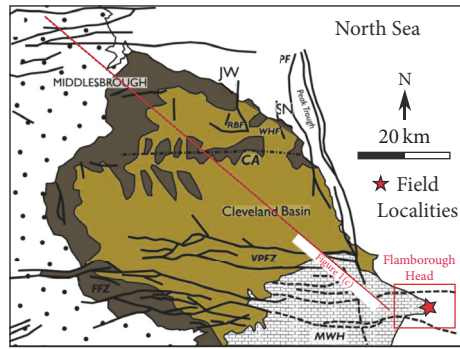
latest Cretaceous till the Neogene and is linked to Alpine orogenic compression from the south and compression related to Atlantic opening to the north. Throughout the Cenozoic, uplift of the basin continued related to the regional tectonic compression, resulting in uplift of the Cleveland Basin and the formation of the Cleveland Anticline [22]. The studied fault outcropping in Selwicks Bay belongs to the Howardian–Flamborough Fault Belt system and is rooted in the basement [12]. The fault thus crosscut the whole stratigraphic section up to the surface (Figure 1).

The Upper Cretaceous chalks of Flamborough Head were deposited as a postrift sediment [19]. The Cleveland Basin is an exhumed potential petroleum system and an onshore analogue of the Southern North Sea Gas Basin. The Cleveland Basin is a Jurassic to early Cretaceous basin, which was inverted during the Cenozoic, at the time of the Alpine Orogeny [24]. It now forms a significant topographic high in the North York Moors. Upper Jurassic syn-rift marine mudstones rich in organic matter (the Kimmeridge Clay Formation) represent the source rocks for most of the region's hydrocarbons [25]. In the North Sea, the whole sedimentary succession, both clastic and carbonate are exploited to extract hydrocarbons, with reservoirs ranging from Devonian to Eocene ages. The Upper Cretaceous Chalk, however, is relatively insignificant as a productive reservoir within the UK sector. The maximal burial depth of chalk deposits ranges from 0.8 to 1.8 km, depending on the authors [26–28]. Structural and petrographic studies in Flamborough Head suggest that chalk experienced several episodes of fracturing related to the tectonic reactivation of basement faults [13, 23, 29]. Selwicks Bay contains a 20 m displacement normal fault characterized by an approximately 10 m wide fault core of breccia and pluridecimeters-thick crystalline calcite veins [13].

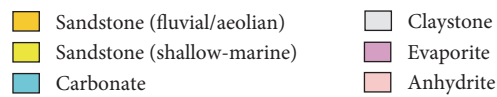
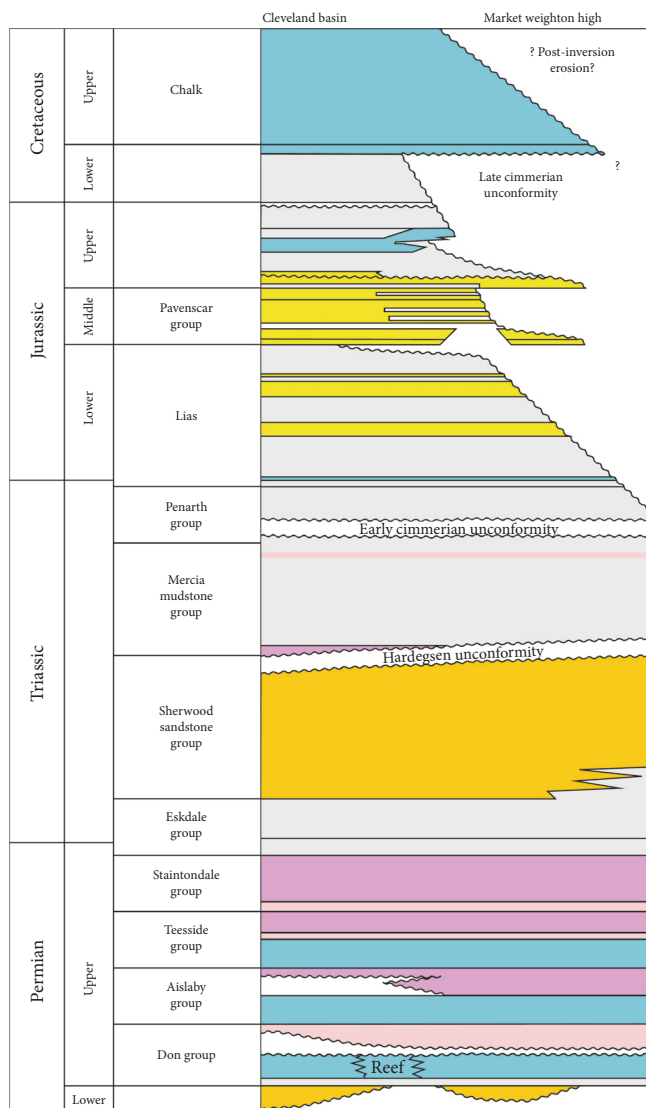
3. Methodology

3.1. Sampling and Petrography. In order to reconstruct the paleofluid evolution, sampling focused on calcite veins, either associated with plurimeters displacement fault damage zones or infilling of centimeter-tick displacement synsedimentary faults. Chalk samples from undeformed host rock were sampled, as well as fragments of chalk from the fault damage zones, in order to allow a petrographic and geochemical comparison. Samples from the protolith are referred to as matrix samples and stratigraphically correspond to the Coniacian-Santonian. Veins crosscutting relationships were first determined in the field, and several samples were taken of each vein generation (Groups I, II, and III). The calcite veins infilling low displacement synsedimentary faults were also sampled. A total of 35 thin sections were studied with standard petrographic methods, employing observations in transmitted light and cold cathodoluminescence microscopy.

3.2. Conventional Geochemistry. Traditional carbon and oxygen stable isotope analyses ($\delta^{13}\text{C}$, $\delta^{18}\text{O}$) were performed on 47 powdered carbonate samples obtained with a microdrill. Samples were analyzed at the Institute of Geology and Mineralogy of the University of Erlangen-Nürnberg (Germany).



(a)



(b)

FIGURE 1: Continued.

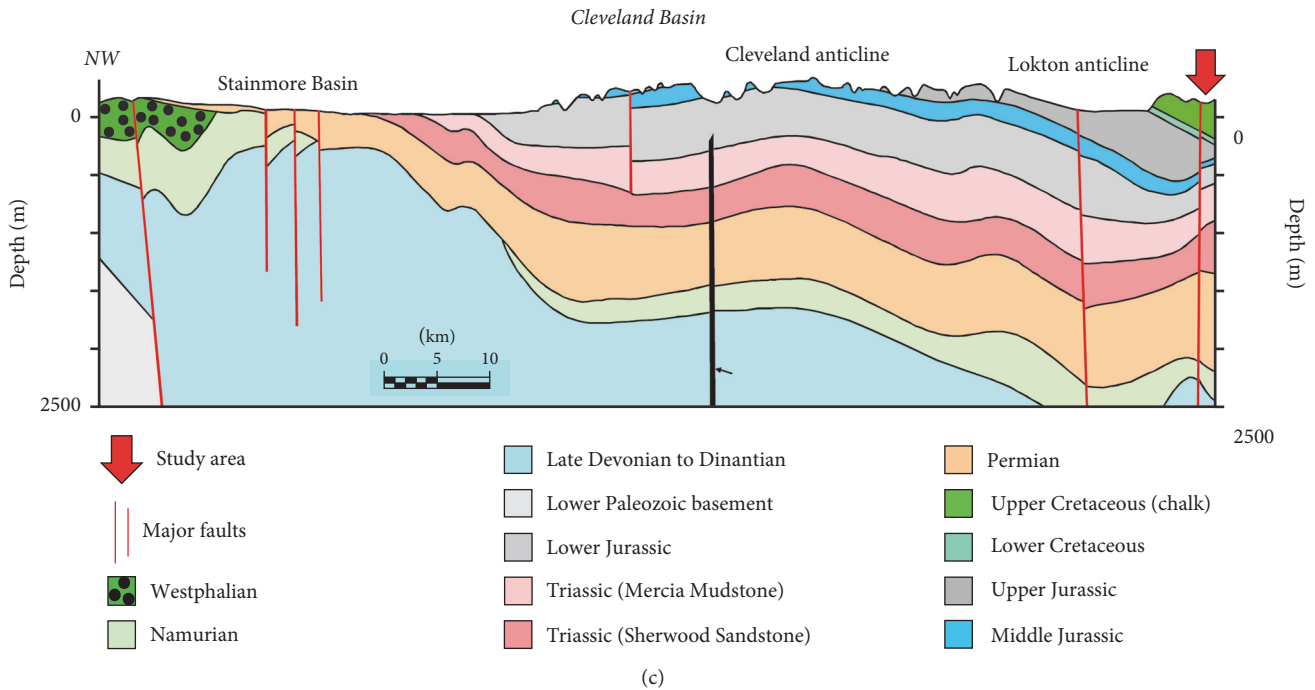


FIGURE 1: (a) Map of the Cleveland Basin, location of the study area and section (c). (b) Cleveland Basin lithology [12]. (c) Cross section of the Cleveland Basin (modified from BGS report [23]).

Powders were reacted with 100% phosphoric acid at 75°C using a Kiel III online carbonate preparation line connected to a ThermoFinnigan 252 mass spectrometer. Isotopic values are reported in the standard δ -notation in per mil relative to V-PDB (Vienna Pee Dee Belemnite). Reproducibility was checked by replicate analyses of laboratory standards and is better than $\pm 0.02\%$ (1σ) for carbon and $\pm 0.05\%$ (1σ) for oxygen isotope.

$^{87}\text{Sr}/^{86}\text{Sr}$ isotope ratio analyses were performed on seven selected samples at the University of Brussels (ULB). Three measurements were performed on the chalk matrix, including both the host rock (2 samples) and chalk fragments from the breccia (1 sample). Four analyses were performed on calcite veins: 1 sample from Group I as well as Group II and 2 samples from Group III. Measurements were performed with a Multicollector Inductively Coupled Plasma Mass Spectrometer (MC-ICP-MS) following the procedure detailed in Snoeck et al. [30]. After measurements, all the raw data were normalized using a standard-sample bracketing method with the recommended value of $^{87}\text{Sr}/^{86}\text{Sr}$ reported for each sample [31]. Strontium concentrations were acquired from small sample fractions (1 to 3 mg) following the procedure described by Weis et al. [31]. Based on repeated digestion and measurement of reference material, the analytical precision (1 SD) of the procedure outlined above is estimated to be below 3%.

A total of 32 representative samples were analyzed for their elemental composition (Mg, Ca, Sr, Fe, Mn, Na, K, Al, Ba, Ni, P, S, Ti, and Zn). Around 50 mg of powdered samples were digested using the so-called 4 acids digestion method, in a Teflon beaker on a hot plate. Samples were

then measured using the Inductively Coupled Plasma Optical Emission Spectroscopy (ICP-OES) Varian 720ES, Varian Inc., Walnut Creek, CA, USA. Analytical error is less than 5%.

3.3. Fluid Inclusion Microthermometry. Double polished 150 μm thick wafers were studied under transmitted and UV-fluorescent light microscopy to select inclusions suitable for microthermometry, following the procedures described in detail by Goldstein and Reynolds [32] and Hurai et al. [33]. The method used for the preparation of the aforementioned double polished sections is described in Muchez et al. [34] and has been proven successful for low-temperature carbonates in a diagenetic system. In order to overcome metastability of the monophase fluid inclusions, samples were put in a freezer at -20°C . This procedure stimulates the formation of vapor bubbles in metastable inclusions without freezing of the samples (e.g., [32]). Measurements were done on a Linkam MDS-600 heating-cooling stage mounted on an Olympus BX51 microscope. The stage was calibrated by synthetic Syn FlicTM fluid inclusion standards. Two-phase aqueous inclusions were heated before freezing in order to obtain the total homogenization temperatures (T_h). Monophase inclusions were artificially stretched by repeated heating of the sample up to 200°C and subsequent freezing to -100°C . These successive cycles caused the formation of larger vapor bubbles. Vapor bubbles which were created by artificial stretching have not been used to determine homogenization temperatures but only for the system (composition, e.g., $\text{H}_2\text{O}-\text{NaCl}$ or $\text{H}_2\text{O}-\text{CaCl}_2$) and the salinity [35]. Subsequent freezing/heating cycles were applied to acquire the first and final ice melting temperatures. All melting temperatures were

recorded in the presence of a vapor bubble, in order to avoid metastable melting [36]. Due to difficulties with the observations related to small inclusion sizes, final melting temperatures of ice have been acquired by sequential freezing [37]. To accurately measure the first and final ice melting temperatures of the fluid inclusions, the stage was heated at a very slow rate (0.2°C per minute). In carbonate rocks, it is common to observe stretching of the inclusions related to the freezing process. Salinities are reported in equivalent weight percent NaCl (eq. wt% NaCl) and were calculated from the temperature of ice melting using the equation of Bodnar [38]. Calculation of the isochores of the aqueous fluid inclusions was carried out using the equation of state of Zhang and Frantz [39].

3.4. Carbonate Clumped Isotope (Δ_{47}) Measurements and Data Processing. The Δ_{47} thermometry is based on the temperature-dependent preference of ^{13}C and ^{18}O isotopes to bond with each other within the mineral lattice at low temperatures. Carbonate clumped isotopes measurements were made at the Institut de Physique du Globe de Paris (IPGP). A detailed description of the analytical setup is given in Bonifacie et al. [40] and is only briefly summarized hereafter. For each analysis, about 5 mg of powdered calcites were digested for 20 minutes in 104% phosphoric acid at 90°C using a common acid bath connected to a vacuum line. The generated gaseous CO_2 is cleaned from traces of water and sulfur or organic compounds before being introduced into the mass spectrometer. The mass spectrometer is a Thermo Fisher MAT 253 operated in dual-inlet mode and configured to simultaneously measure masses 44 through 49 of the sample CO_2 versus a working reference gas provided by Oztech Trading Corporation (with $\delta^{18}\text{O} = -15.79\text{‰}$ and $\delta^{13}\text{C} = -3.63\text{‰}$; verified through measurements of the international reference material NBS 19). Each measurement consists of 1820 seconds per analyses at a signal of 12 V on mass 44. Carbonate clumped isotope composition (Δ_{47}) is defined as the excess of mass 47 in the analyzed CO_2 relative to what it should be if ^{13}C and ^{18}O isotopes were randomly distributed between all CO_2 isotopologues. Δ_{47} data are here referenced to the absolute reference frame (or CDES for Carbon Dioxide Equilibrated Scale) of Dennis et al. [41] using empirical transfer functions (ETF). ETF were built with multiple analyses of different CO_2 gases (with $\delta^{13}\text{C}$ and $\delta^{18}\text{O}$ values covering the range of the unknown samples) that were brought to thermodynamic equilibrium at either 1000°C or 25°C and analyzed interspersed with carbonate standards and unknown samples. As our samples were digested at 90°C, an acid correction factor of 0.082‰ (following [42]) was added in order to report the data in a 25°C acid digestion frame to follow the common use. All samples were analyzed three times in three discrete analytical sessions separated by several weeks (i.e., with ETF correction frames constructed with various sets of data on CO_2 standards equilibrated at known temperatures) in order to eliminate possible bias from potential error in constructing one of the three discrete correction frames. To ensure accuracy of Δ_{47} data and the entire data reduction process described above, we routinely

analyzed two carbonate reference materials (Carrara marble and 102-GCAZ01b, also reported by Dennis et al. [41] and many other studies) distributed along the unknown samples in all runs. The standard deviations of carbonate reference materials are typically of $\pm 0.014\text{‰}$, consistent with long-term external reproducibility for Δ_{47} measurements at IPGP (1 SD, $n > 300$; [40, 43]). Traditional $\delta^{18}\text{O}$ and $\delta^{13}\text{C}$ data were acquired as part of each Δ_{47} analyses and ^{17}O corrections were made using the ^{17}O parameters from Santrock et al. [44]. In order to account for the temperature dependence of oxygen isotope fractionation between CO_2 gas and calcite resulting from the reaction with phosphoric acid at 90°C in a common acid bath, a fractionation factor of 1.00811 was used [43].

The Δ_{47} data were converted into temperatures using the interlaboratory composite Δ_{47} - T calibration recently published for all carbonate minerals with crystallization temperatures ranging from -1°C to 300°C [40]. Because any Δ_{47} measurement comes with simultaneous determination of the oxygen isotopic composition of the analyzed carbonate ($\delta^{18}\text{O}_{\text{carb}}$), Δ_{47} thermometry provides independent estimates of the carbonate formation temperature and of the oxygen isotopic composition of the mineralizing fluid ($\delta^{18}\text{O}_{\text{water}}$). $\delta^{18}\text{O}_{\text{water}}$ was calculated using the equation of oxygen isotope fractionation between calcite and water from Kim and O'Neil [45].

4. Results

4.1. Petrography

4.1.1. Macroscopic Observations. A normal fault was studied at Selwicks Bay, striking ENE-WSW, and dipping steeply ($\text{N}70^\circ$) to the NNW. The fault zone is characterized by calcite cementation and presence of cemented brecciated zones [13, 14]. The main fault core forms a 5 m wide promontory on the cliffs. The damage zone of the fault is characterized by a much higher density of calcite veins compared to the surrounding wall rocks. The intensity of calcite veining reduces progressively when moving further away from the fault core zone. In the core zone of the main fault at Selwicks Bay, field observations evidenced three generations of calcite veins; namely,

- (i) Group I veins correspond to thin crack and seal like veins, characterized by a network of mostly parallel thin veins measuring a few micro- to a few millimeters wide. They are oriented perpendicular to stratigraphy. In some places, the stratigraphy is tilted, and veins of Group I are oriented perpendicular to the stratigraphy, indicating that veins occurred prior to the tilting. Group I veins usually crosscut compaction stylolites (Figure 2(a)) but are sometimes crosscut by the latter (Figure 2(b));
- (ii) Group II veins consist of a breccia with angular rock fragments healed by calcite cement. Clasts are composed of chalk and occasionally chert with sizes ranging from millimeter to decimeter (Figures 2(c)–2(e)). Both the angular shape of the fragments

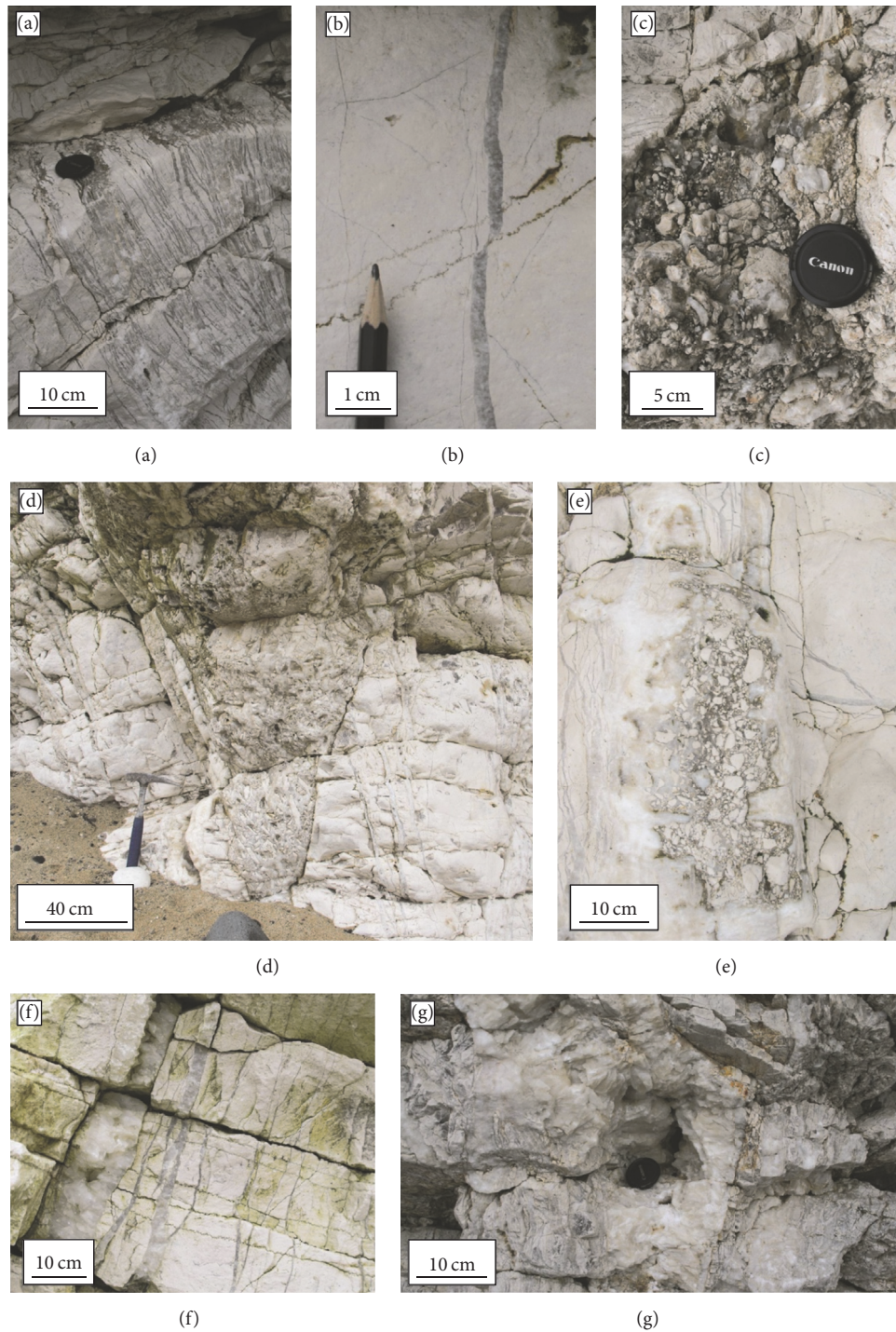


FIGURE 2: Macroscopic observations of the calcite veins. (a) Group I vein generation characterized by a network of pseudo parallel thin veins. (b) A vein from Group I crosscut and displaced by a compaction stylolite. (c) Hydraulic breccia and its typical jigsaw texture. (d) Hydraulic breccia crosscutting the stratigraphic section and compaction stylolites. (e) Hydraulic breccia (with Group II veins) intruded by Group III vein (bright white color). (f) Group III vein crosscutting compactional stylolites. (g) Large calcite crystals infilling porosity along the main fault plane (Group III veins).

and the jigsaw puzzle configuration reflect a limited transport, in conjunction with fast crystallization pointing towards a hydraulic type of fracturing. Chalk fragments include Group I veins, constraining the relative chronology of the vein generations;

- (iii) Group III veins are to the last vein generation identified. Veins III crosscut the hydraulic breccia. They are characterized by a bright white color and large calcite crystals. In the main brecciated zone, calcite crystals up to tens of centimeters in width fill up the macroporosity in the vicinity of the fault plane (Figures 2(f) and 2(g)).

Within the Flamborough Head area, on both sides of Selwicks Bay fault, decimeter to few meters long bed-confined normal faults are present. They are part of the polygonal fault systems described by Fay-Gomord et al. [7], which include fault systems of different scales from centimetric to decametric. Some of those faults are cemented. Calcite cementation is observed in the south of South Landing and north of Thornwick areas, up to 1 km away from Selwicks Bay fault. These veins were also sampled and referred to as chalk confined fault (CCF) veins. Some of these faults were reactivated as tectonic stylolites, displaying indentation parallel to the stratigraphy associated with N-S compression.

4.1.2. Microscopic Observations. Thin-section petrography confirmed the crosscutting relationships established during field observations. Group I veins consist of calcite crystals, usually ranging in size between 10 and 50 μm (Figures 3(a)–3(c)). They display mutual crosscutting relationships with bedding-parallel stylolites. The hydraulic breccia cement (Group II veins) is characterized by sparitic calcite crystals measuring usually several 100 μm . Cement commonly displays a drusy mosaic texture (Figure 4(b)), whereby crystal size increases from the border of the chalk fragments towards the centers of the veins. Impurity fringes are commonly observed along chalk fragments in the hydraulic breccia and also contain rhombohedral dolomite crystal ghosts (Figures 3(b) and 3(c)). Dolomite ghosts measure 50 to 150 μm wide, and their porosity is either preserved or partially filled by micrite. Cathodoluminescence images show growth zonations within certain sparry calcite crystals, but dull to nonluminescent sector zonations are mostly observed (Figure 4). Group III veins have calcite cement with two different crystal morphologies, namely, (1) euhedral crystals growing perpendicular to vein walls and (2) crystals of subhedral to anhedral blocky calcites with no specific orientation. Cathodoluminescence analyses also revealed sector zonations within some of the blocky calcite crystals of the last vein generation. Twinning planes with crossing angles of about 60° are observed in some sparitic crystals of Group II and III veins.

4.2. Conventional Geochemistry

4.2.1. Stable Isotopes. Oxygen and carbon isotope ratios were measured on both matrix and vein samples taken from host chalk rock and calcite-filled fractures. All matrix samples

display similar $\delta^{18}\text{O}$ (from -4.78 to -3.30‰) and $\delta^{13}\text{C}$ values (from $+2.00$ to $+2.57\text{‰}$) (Figure 5). The stable isotope values of the vein samples define a second cluster, with $\delta^{18}\text{O}$ values of vein samples ranging from -7.27 to -9.01‰ , with no distinction between the different vein generations. $\delta^{13}\text{C}$ signatures of veins range from -2.19‰ to $+2.89\text{‰}$, with no distinction between vein generations either.

4.2.2. Strontium Isotopes. The $^{87}\text{Sr}/^{86}\text{Sr}$ ratios in matrix chalk samples range from 0.7074 to 0.7075. The results are in good agreement with the Upper Cretaceous marine carbonate signal (0.7073–0.7076) reported by Mearon et al. [46]. The $^{87}\text{Sr}/^{86}\text{Sr}$ ratios obtained in veins display values significantly higher. $^{87}\text{Sr}/^{86}\text{Sr}$ equals 0.7103 in the sample of Group I vein generation, 0.7085 in the cement of the hydraulic breccia (Group II), and 0.7103 in the last vein generation (Group III).

4.2.3. Trace Elements. The elemental concentrations are shown in Table 1. The chemical compositions of the host rock and the veins display very distinct signatures. Veins, independently of their generation (e.g., Groups I, II, and III), exhibit low concentrations of trace elements. Chalk matrix samples generally show higher Al, Fe, and K content than the calcite veins, while no significant differences in Ca and Mg concentrations are observed. The Al and K contents relate to the presence of noncarbonate constituents, especially clays in the chalk. The high Fe and S concentration of the chalk may be associated with the presence of some pyrite in the matrix. Fe concentration equals 491 ppm on average for matrix samples. Veins are characterized by significantly lower Fe concentrations, with Group II and III veins displaying the lowest Fe concentration (110 ppm on average) and Group I veins with higher values (232 ppm on average). The geochemical signature of the CCF veins, infilling the polygonal fault systems is very similar to Group I and II veins.

4.3. Fluid Inclusion Microthermometry. Numerous aqueous fluid inclusions displaying various degree of deformation are identified along the crystal growth planes (Figure 6). The fluid inclusions selected for measurements are primary in origin and show no indication of stretching, necking down, or deformation. Optical and fluorescence microscopy revealed that most inclusions are monophasic aqueous inclusions. Few fluid inclusions are two-phase aqueous inclusions, which range in size from ~ 8 to 12 μm , with a relatively constant liquid : vapor ratio. The monophasic liquid aqueous inclusions range from a few microns to $\sim 10 \mu\text{m}$ and are interpreted to have been entrapped below $\sim 50^\circ\text{C}$ (cf. [32]). Monophasic inclusions which still show no vapor bubble development after cooling up to -20°C in a freezer are most likely not metastable (Muecher & Slobodnick, 1996).

Difficulties with the measurement of the first melt temperature are explained by the limited amount of hydrohalite and ice that melt at the eutectic temperature (T_e) of -21.2°C , in combination with a small inclusion size. The first melt related observations made below T_e is the appearance of rounded ice crystals with a fluid in between them. Freezing

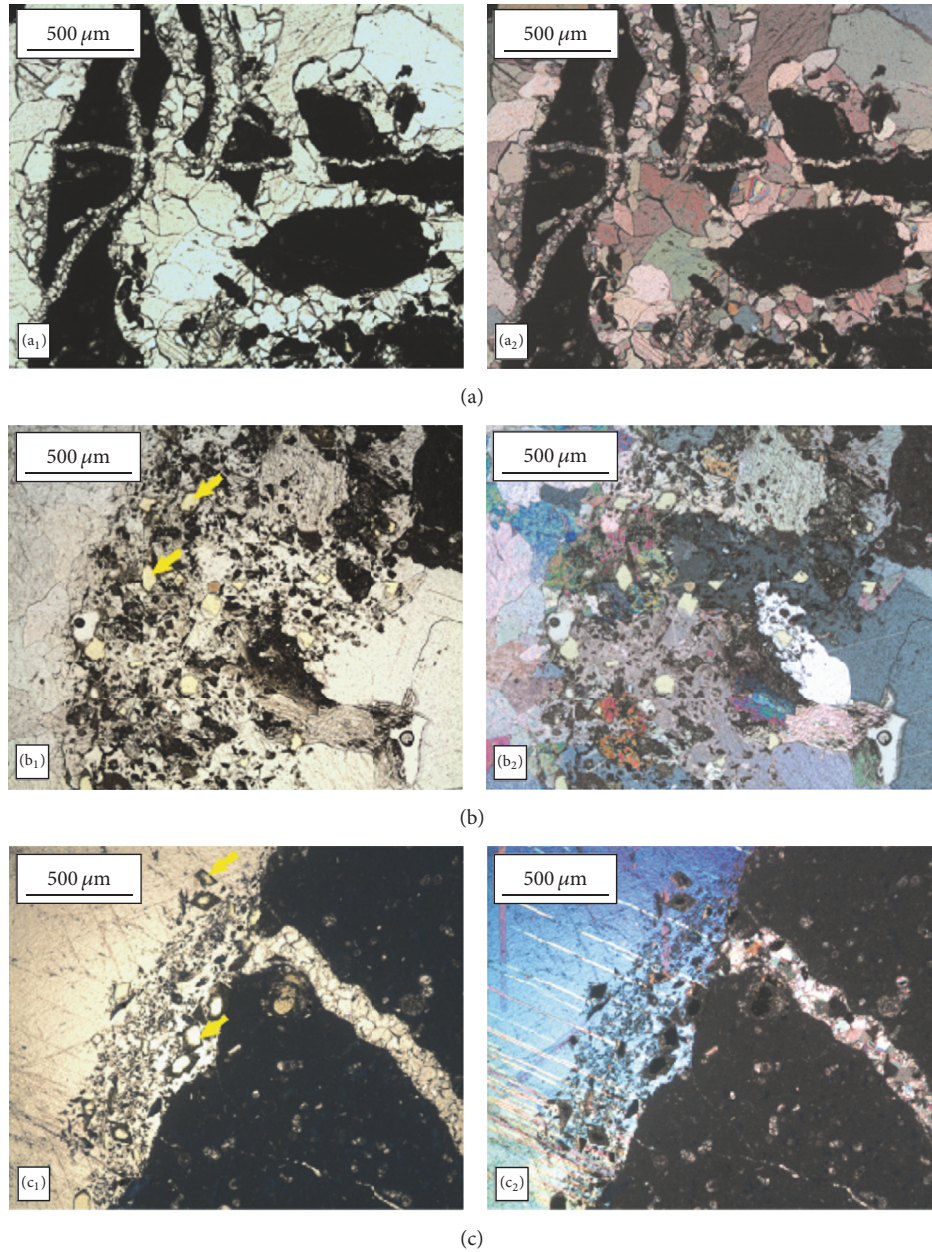


FIGURE 3: Microscopic observations under plane-polarized transmitted light (1) and crossed polars (2). (a) Calcite-cemented breccia (Group II) with chalk fragments showing a typical jigsaw puzzle. Group I veins within chalk fragments. (b) and (c) Fringe of impurities along a chalk fragment within the calcite-cemented breccia. Note the rhombohedral crystal ghosts (yellow arrow).

behavior shows additional evidence for a relatively low saline H₂O-NaCl system. The temperature of metastable freezing (T_{fr}) is observed by an instantaneous volume decrease, deformation, or jump in bubble position. This “jerk” or “collapse” of the vapor bubble, in the observed temperature range of -34°C to -50°C , is typical behavior for H₂O-rich inclusions (Roedder, 1984). The aforementioned range in T_{fr} measurements can be explained by salinity and inclusion size variations [47].

Group I veins do not contain any fluid inclusions large enough for microthermometric analyses.

Group II veins (e.g., hydraulic breccia cement) are characterized by homogenization temperatures ranging from 34 to 48°C . The temperature of first melting is difficult to observe and the lowest values are below -10°C . The final melting temperatures range from -7.2 to -0.1°C . Using the equation of Bodnar [38] and assuming a H₂O-NaCl system based on the freezing temperatures (T_{fr}), the final melting temperatures correspond to a salinity ranging from 0.3 to 10.7 eq. wt% NaCl.

The homogenization temperatures of inclusions in Group III veins are between 37 and 53°C . The temperature of first

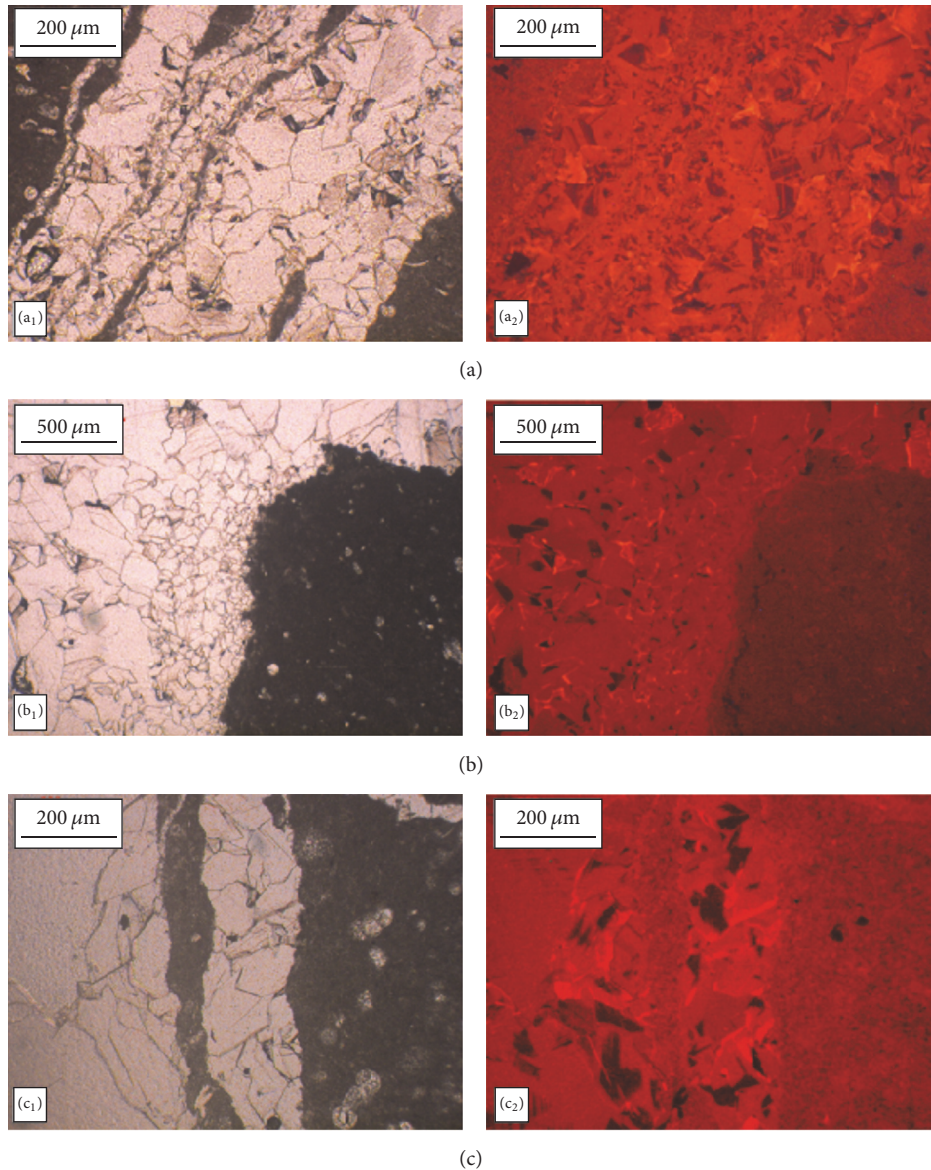


FIGURE 4: Microscopic observations under plane-polarized transmitted light (1) and cathodoluminescence (2). (a) Group I veins with visible sector zonation. (b) Hydraulic breccia cemented by drusy calcite cement. (c) Group I veins with sector zonation visible under cathodoluminescence.

melting is difficult to observe and is below -7°C . Within a $\text{H}_2\text{O}-\text{NaCl}$ system, based on the final melting temperatures, ranging from -4.6 to -0.1°C , the calculated salinities range from 0.2 to 7.3 eq. wt% NaCl.

All vein generations display similar homogenization temperatures and a range of salinity values. Most salinity values are below 1 eq. wt% NaCl and reflect a meteoric water signal, as shown in Figure 6(c). The spread of values between a meteoric signal and 10 eq. wt% NaCl could be due to the mixing of meteoric water with a saline fluid or to the dissolution of evaporites.

The average homogenization temperature measured is 45°C . Using a temperature of 45°C and two different salinity values of, respectively, 7.7 and 0.4 eq. wt% NaCl, the isochores

of the latter two fluids have been constructed in a P-T diagram (Figure 6(d)). The burial depth is estimated around 1 km since veins crosscut compaction stylolites and are crosscut by compaction stylolites, formed from a depth of ~ 800 m in chalk [48]. Using the appropriate isochores (lines of equal density) and a typical hydrostatic pressure of 10 MPa/km, calculated trapping temperatures are 52 and 53°C . Using a typical lithostatic pressure gradient of 25 MPa/km for the same samples, calculated temperatures are 60 and 62°C .

4.4. Temperature and $\delta^{18}\text{O}_{\text{water}}$ from Δ_{47} Data. Data obtained from clumped isotope measurements on three carbonate groups are reported in Table 2. For one analyzed sample, the three Δ_{47} measurements are showing external

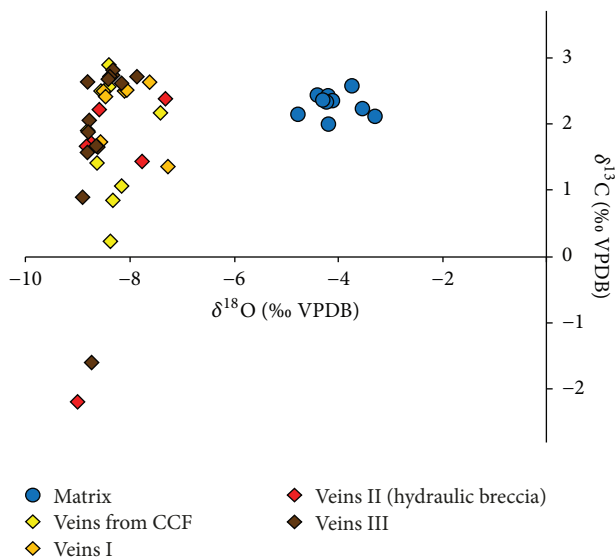


FIGURE 5: $\delta^{13}\text{C}$ versus $\delta^{18}\text{O}$ cross plot of the calcite veins and chalk matrix (host rock and breccia fragments) from Flamborough Head (UK). Matrix and veins display distinct signatures, while different vein generations display similar signatures.

reproducibilities that are consistent with the $\pm 0.014\text{‰}$ long-term external reproducibility obtained on homogeneous carbonate standards over several years of analyses. This attests to the homogeneity of the samples and the good quality of the isotopic measurements, with three groups showing an average Δ_{47} value of $0.588 \pm 0.012\text{‰}$ ($n = 3$ samples and 9 measurements). The latter suggests indistinguishable formation temperature (average temperature of $60 \pm 5^\circ\text{C}$, 1 SD), for the three samples from each vein generation. The calculated $\delta^{18}\text{O}_{\text{water}}$ values of the three samples are also indistinguishable within uncertainty, with average values of $0.5 \pm 0.9\text{‰}$ (1 SD).

5. Discussion

5.1. Origin of the Fluid. Several pulses of fluid flow were identified based on the crosscutting relationships, as confirmed by the petrographical analyses. Nevertheless, similar trace element and isotopic compositions of the different vein generations reveal one common fluid source. The strontium isotopic composition of the veins possesses a radiogenic signal, which does not match that of the Upper Cretaceous seawater. The high $^{87}\text{Sr}/^{86}\text{Sr}$ ratio is probably related to the interaction of the fluid with minerals containing radiogenic ^{87}Sr . Enrichment in ^{87}Sr may occur when the mineralizing fluid had been in contact with siliciclastic aquifers. Trace element analyses, which revealed a low concentration of Fe or Mn in the calcite veins, suggest that the aquifers were probably composed of sandstones. The spread of salinity values measured by microthermometry analyses supports a dominant meteoric origin of the fluid, which has either been mixed with saline fluids or enriched in salt due to the dissolution of evaporitic minerals. In the Cleveland Basin,

the Sherwood Sandstone Group represents an aquifer, up to 450 m thick [49], which belongs to the Permo-Triassic sandstones group, the second most important aquifer in the UK [50]. If the infiltration area of the Sherwood Sandstone aquifer is located hundreds of kilometres away, the Sherwood Sandstone Formation is still present just 1 km below the chalk in the study area (Figure 1). The Sherwood Sandstone Group forms the most important aquifer in Northern England and the meteoric water migrated in the formation far away from the recharge area as reported in several papers. A number of large towns obtain their water supplies at least partly from the Permo-Triassic sandstones, among them are Manchester, Liverpool, Birmingham, Leeds, Doncaster, and Nottingham [51]. The sedimentology and diagenesis of the Sherwood sandstones have been widely studied: Burley [52] addressed the composition of the sandstone reservoir which contains several Sr-bearing minerals, including plagioclase feldspars, as well as igneous and metamorphic rock fragments. Worden et al. [53] described highly saline formation waters within the Triassic Sherwood Sandstone of the Wessex Basin and suggested that a meteoric fluid became enriched in salt due to the dissolution of evaporites. The lithostratigraphy of the Cleveland Basin reveals the presence of halite deposits, both underneath the Permo-Triassic sandstones and interbedded within the Upper Triassic Mercia Mudstone Group, which overly and confine the Sherwood sandstones (Figure 1(b)). The latter is considered the most probable source of salt within the Sherwood Sandstone aquifer [53].

Fluid inclusion microthermometric analyses display salinity values supporting dominantly meteoric water. Nevertheless, the $\delta^{18}\text{O}_{\text{water}}$ value of the mineralizing fluid calculated from clumped isotope measurements range from -0.2 to 1‰ , while the meteoric water signature usually ranged from -3 to -10‰ (SMOW) at the corresponding latitude from the Permian to Late Cretaceous [54]. If the fluid remained stored in an aquifer for sufficiently long time period, it is probable that $\delta^{18}\text{O}_{\text{porewater}}$ reflects an extended water-rock interaction under low fluid to rock ratio [55]. In addition, some samples display low $\delta^{13}\text{C}$ values and two samples especially possess negative values, which probably reflect interference from a depleted source.

The diagenesis of the Sherwood Sandstone has been described from several locations throughout the UK, the Irish Sea, and the North Sea (e.g., [52, 56, 57]). Deep burial diagenetic processes led to the precipitation of different cement phases, including ankerite and anhydrite cements, which represent several percentages of the total bulk rock volume, occasionally reaching up to 17% [54, 58, 59]. These cements, which overgrow previous mineral phases, reportedly yield original $\delta^{18}\text{O}_{\text{water}}$ (SMOW) values ranging from 0 to 5‰ (2‰ on average) [54]. Ankerite precipitation in the Sherwood Sandstone probably led to iron depletion in the formation water of the Sherwood Sandstone. The water could have been remobilized during tectonic reactivation giving rise to the cementation of calcite veins within the Chalk. This hypothesis could also explain the low iron concentrations measured within the calcite veins (200 ppm on average), which also yield a radiogenic signal.

TABLE 1: Trace elements concentrations measured by ICP-OES.

	Ca %	Al μg/g	Ba μg/g	Fe μg/g	K μg/g	Mg μg/g	Mn μg/g	Ni μg/g	P μg/g	S μg/g	Sr μg/g	Ti μg/g	Zn μg/g
LOQ	0.8	20	1	20	10	10	0.2	1	15	20	15	1	2
Matrix	37	1172	12	492	356	1661	418	25	225	246	970	45	15
1	37.2	1134	10	431	368	1567	436	6	210	344	923	40	11
2	38.4	1163	13	387	269	1511	436	-	289	254	998	34	21
3	37.4	968	10	439	317	1617	481	12	328	270	917	33	16
4	37.4	1291	13	601	398	1717	461	6	192	207	1098	54	14
5	36.3	1409	12	598	518	1795	421	31	203	343	1036	56	13
6	38.4	481	9	322	151	1609	258	79	151	152	793	15	17
7	37.3	1761	15	663	468	1813	436	15	199	151	1028	80	15
CCF veins	39	72	44	213	30	1350	413	1	12	44	1229	3	2
8	38.9	87	5	75	31	1457	312	2	18	37	1147	4	2
9	38.8	45	1	770	17	1433	327	2	6	29	777	1	2
10	38.6	115	6	304	48	1430	413	1	14	32	1907	7	4
11	38.6	83	3	26	31	1697	404	-	19	23	1972	3	2
12	38.9	62	5	331	32	1408	404	0	16	33	1613	2	2
13	38.6	112	7	47	46	1307	424	1	15	42	1597	4	2
14	38.7	43	322	37	22	951	496	0	2	118	373	1	2
15	38.8	29	3	114	16	1115	522	0	3	40	447	1	1
Group I veins	39	275	5	233	106	1504	402	35	48	159	1309	11	4
16	38.6	185	3	125	60	1304	433	-	63	113	951	6	-
17	41.7	144	4	389	96	1614	428	19	21	236	1598	7	-
18	39.0	38	2	59	18	1389	283	21	9	17	958	1	1
19	38.1	355	9	370	134	1655	426	125	58	145	1602	11	6
20	38.0	346	6	277	137	1488	431	4	67	359	1151	13	5
21	38.3	584	5	176	190	1571	410	4	70	84	1595	28	4
Group II veins	39	229	11	100	78	1540	494	10	57	86	1349	11	-
22	38.6	146	5	53	68	1435	429	17	39	115	1667	7	-
23	39.3	312	17	146	88	1644	559	3	74	56	1030	14	-
Group III veins	39	52	6	79	31	1601	444	13	17	42	1495	8	3
24	38.9	49	5	-	57	1609	473	29	-	54	1474	3	-
25	38.9	56	6	35	33	1567	471	30	20	85	1415	3	-
26	38.6	-	2	41	19	1484	436	-	-	-	1429	-	-
27	39.0	-	2	341	-	1435	462	15	-	-	944	49	-
28	38.8	35	6	16	18	1753	449	8	18	31	1702	1	3
29	38.5	28	6	23	29	1751	447	12	18	24	1698	1	6
30	37.1	58	6	125	29	1572	437	0	9	33	1151	5	2
31	40.1	66	17	26	34	1679	413	-	25	39	2357	2	1
32	38.6	69	2	28	27	1555	410	0	10	27	1286	2	2

CCF: chalk-confined fractures, “-”: values below detection limit; LOQ: limit of quantification.

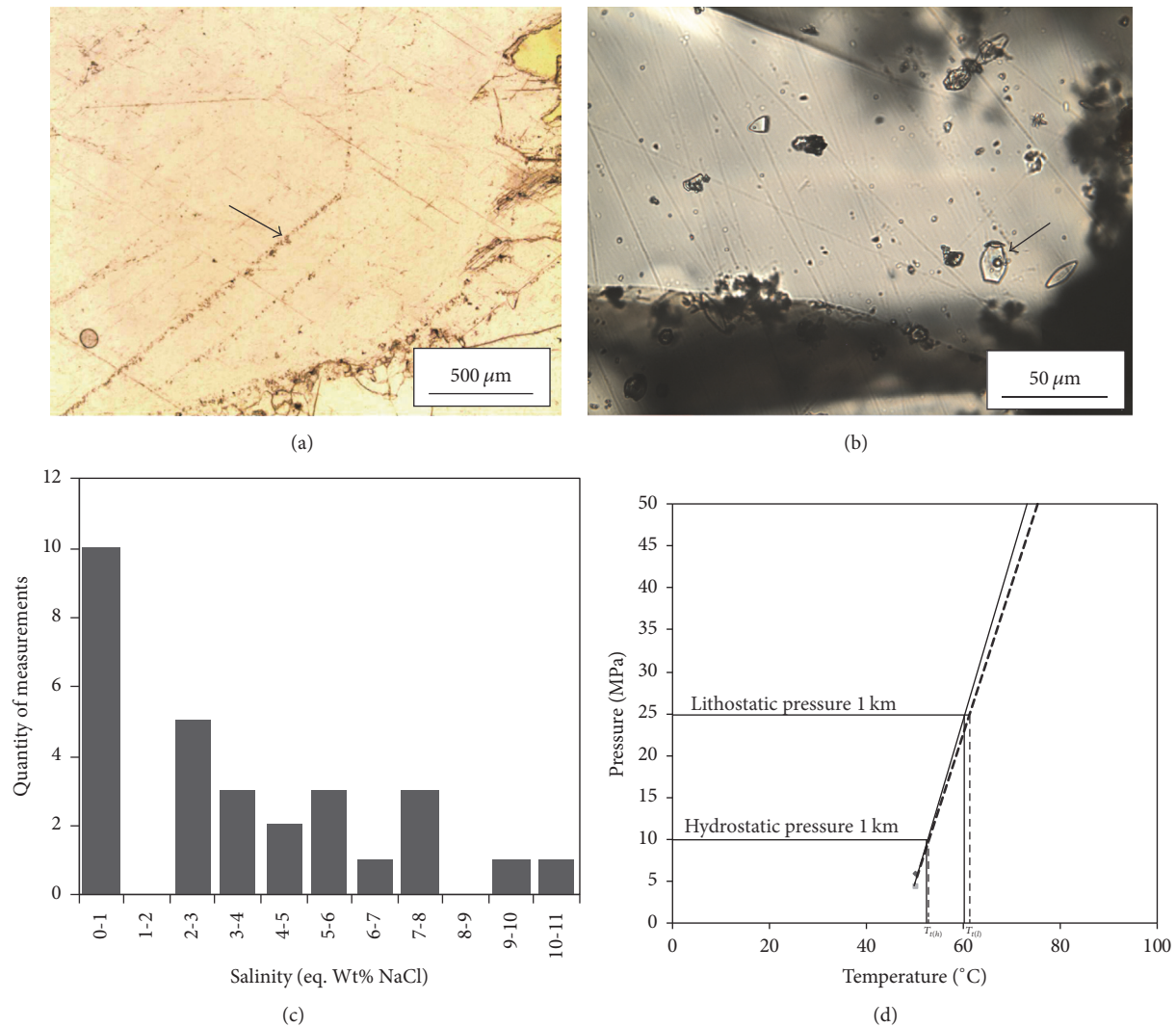


FIGURE 6: Synthesis of the fluid inclusions data. (a) Optical microscopy observation of inclusions arranged along crystal growth planes (arrow). (b) Zoom-in on a two-phase aqueous inclusion (arrow). (c) Distribution of the salinity values calculated from microthermometry. (d) Pressure-temperature diagrams and isochores of a low salinity system (full line) and an intermediate salinity system (dashed line) and estimated trapping temperature (T_t) assuming a 1 km hydrostatic or lithostatic pressure.

5.2. Relative Timing of Events and Evolution of Fluid Flow. The diagenetic processes affecting the Flamborough Chalk deposits are summarized in Figure 8 and are shown in relation to the regional burial history diagram proposed by Emery [23].

Early Faulting and Fluid Flow Event. The petrographical study of the breccia revealed a large number of impurities and rhombohedral crystal ghosts, concentrated in clusters along one side of some chalk fragments. Crosscutting relationships with calcite sparitic cement (Vein Group II) show that the impurities-rich fringes predate vein cementation. The presence of rhombohedral ghosts suggests the formation of dolomite rhombs prior to the breccia cement mineralization. A possible source of Mg necessary for dolomite precipitation could be related to smectite-illite recrystallization processes.

Smectite minerals are converted to ordered smectite-illites as temperatures increase with burial depth, releasing free ions in solution. In the Cleveland Basin, the Chalk Group is underlain by a hundred meters thick succession of clays and clay-rich deposits. Previous studies demonstrated that the Lower Jurassic Whitby Mudstone Formation [60], the Lower Cretaceous Speeton Clays [61, 62], or the Upper Jurassic Oxford and Kimmeridge clays [63, 64] contain illite-smectite (I-S) mixed layer clays with up to 90% illite. The overpressure created by the smectite to illite conversion in the Cleveland Basin may have led to fluid migration into the overlying lithologies [65], including the Chalk. We suggest Mg^{2+} enriched fluids migrated along the main fault zone and within the preexisting connected fault system of the chalk, resulting in the crystallization of dolomite rhombs in veins along fault planes. The migration of this fluid predates the

TABLE 2: Data from clumped isotopes analyses.

	$\delta^{13}\text{C}$ (‰, VPDB)	$\delta^{18}\text{O}$ (‰, VPDB)	Δ_{47} (‰, CDES)	Av. Δ_{47} (‰, CDES)	± 1 S.D. (‰)	T. (°C)	$\delta^{18}\text{O}_{\text{water}}$ (SMOW)
Sample Group I	2.54	-7.74	0.582	0.588	0.012	60 ± 3	1.0 ± 0.8
	2.56	-7.74	0.581				
	2.54	-7.69	0.602				
Sample Group II	2.61	-8.21	0.595	0.597	0.004	56 ± 3	-0.1 ± 0.2
	2.47	-8.19	0.601				
	2.60	-8.25	0.594				
Sample Group III	0.75	-8.79	0.577	0.579	0.016	64 ± 4	0.6 ± 1.2
	0.81	-8.78	0.596				
	0.79	-8.71	0.565				

For each sample the three Δ_{47} replicate measurements are averaged and show one standard deviation close to that found for homogeneous carbonate standards ($\pm 0.014\%$, 1 SD). Uncertainties on temperature estimates are calculated from this $\pm 0.014\%$ external reproducibility or the SD obtained here if higher. Uncertainties on $\delta^{18}\text{O}_{\text{water}}$ values reflect the variability in $\delta^{18}\text{O}_{\text{carb}}$ and Δ_{47} values.

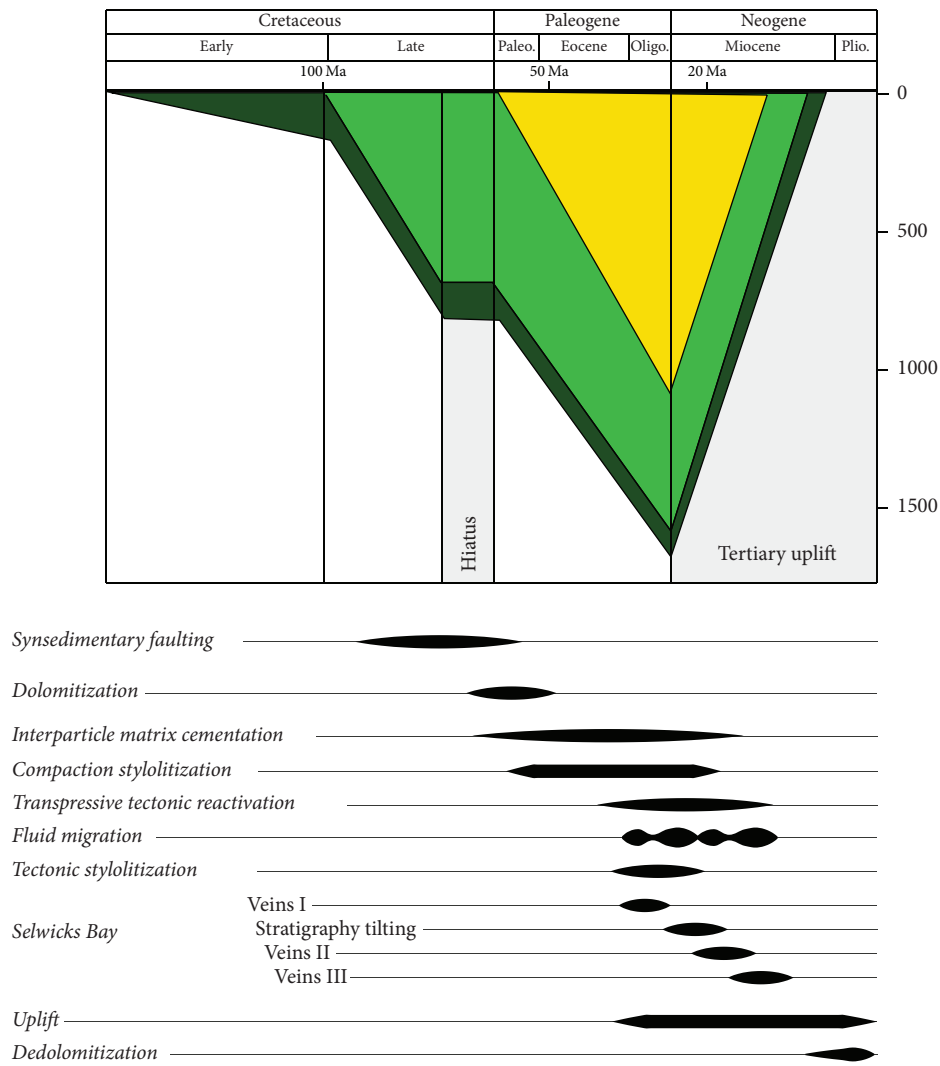


FIGURE 7: Relative timing of the diagenetic and fluid flow events affecting Chalk deposits in Flamborough Head (UK).

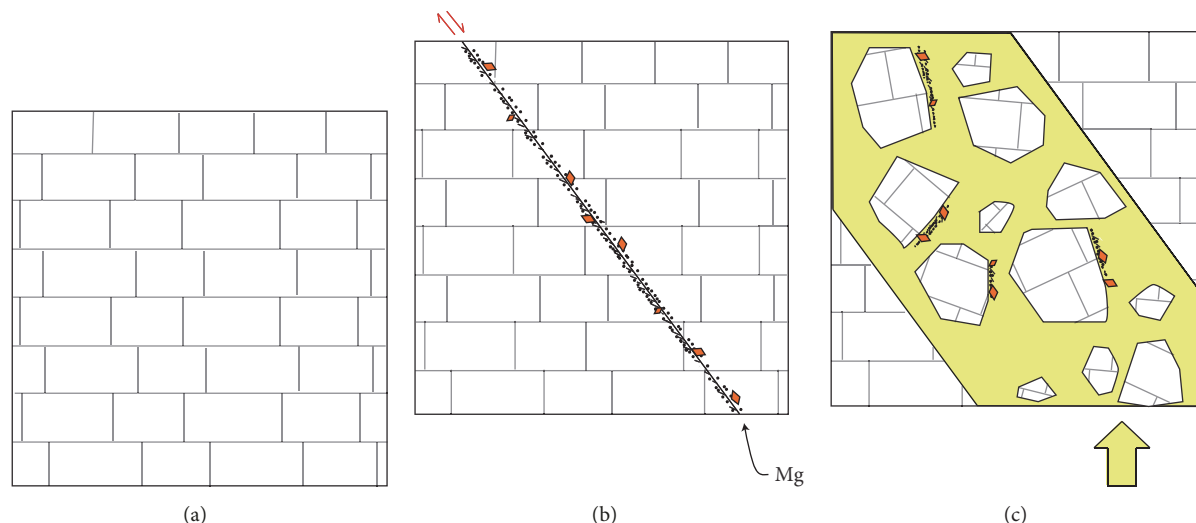


FIGURE 8: Schematization of the different phases of fluid flow within the chalk succession. (a) Chalk sedimentation. (b) Early synsedimentary fractures, fluid circulation probably coming from the compaction of underlying clays (Lower Cretaceous and Upper Jurassic) and associated dolomitization. (c) Late Cretaceous tectonic reactivation and fluid circulation likely coming from the Sherwood Sandstone and resulting in breccia formation.

principal fluid flow event that led to the brecciation and extensive calcite mineralization (Figure 7).

Burial Diagenesis and Matrix Cementation. Within chalk deposits, burial diagenesis resulted in pressure solution processes taking place along stylolitic planes. Safaricz and Davison [66] estimated that 40% of the initial volume of chalk was lost due to chemical compaction. They estimated that dissolution of 30 mm thick of chalk results in a 1 mm thick of insoluble residue seam. A large number of marl-seams and stylolites imply that 100s m of chalk was dissolved from the whole Coniacian-Campanian chalk. Chalk insoluble residue of Coniacian-Campanian chalk is lower than 5% so a high amount of dissolution is required to accumulate few millimeters of insoluble residue. The dissolution resulted in reprecipitation within the micritic matrix, as interparticle cement, thus affecting matrix porosity and permeability, with respective values as low as 8% and 0.04 mD [67]. Compaction stylolite planes, resulting from pressure solution, do not display any evidences of fluid circulation such as calcite cementation. In addition, $\delta^{18}\text{O}$ of the sea from the ice-free Late Cretaceous sea is estimated at -1.2‰ [68]. The calculated $\delta^{18}\text{O}_{\text{water}}$ of the fluids from which calcite veins precipitated range from 0 to 1‰. This provides an additional argument to support the fact that chalk is probably not the aquifer providing the mineralizing fluid, backing up the solid radiogenic Sr-isotope signal. At such low temperature, however, the isotope fractionation is probably kinetic and equilibrium may not have been reached, thus bringing an uncertainty to the calculated data.

Late Cretaceous Inversion: Fluid Flow and Hydraulic Fracturing. A phase of basin inversion occurred at the end of the Late Cretaceous-Early Cenozoic [24]. It affected many basins in

NW Europe, including the Sole Pit Basin and the Cleveland Basin (Figure 1). Postburial structural inversion, particularly in shallow burial basins and at basin margin, allowed the reintroduction of meteoric water into the Sherwood Sandstone [52]. Bedding-parallel hydraulic fractures were reported in the Lower Jurassic shales of the Cleveland Basin [23] and Mesozoic mudstones and shales from the Wessex Basin [69]. In both cases, the timing of their formation was related to the Late Cretaceous to Cenozoic tectonic inversion. In Selwicks Bay, the tectonic inversion led to folding and tilting of the stratigraphy [13]. Some normal faults were reactivated during the inversion. Along the south coast of Flamborough (e.g., South Landing) only a preferential E-W orientation of the polygonal fault system was reactivated during the NNW-SSE compression and transpression events (described by Starmer et al., 2013). Many of the faults oriented perpendicular to the compression were reactivated as vertical stylolites. In Selwicks Bay, crosscutting relationships demonstrated that the tilting essentially occurred between Group I and Group II veins. Successive vein generations were identified in the field and geochemical analyses revealed that they originated from the same kind of fluid. The consecutive fluid flow events could be related to pulsating phases of inversion, which started during the Campanian and ended with the Laramide pulse of intraplate compression during Paleocene-Eocene [70].

Fluid flow under high pressure led to the formation of cemented breccia resulting from hydraulic fracturing [17]. Part of the overpressure may relate to the tectonic stress regime at the time, involving both the Alpine Orogeny and the Atlantic opening [23]. Nevertheless, previous studies [23, 69] suggest that tectonic forces alone do not allow reaching pore pressures high enough to initiate hydraulic fracturing, and the role of source rock maturation and oil generation was demonstrated. Our petrographical study

including both fluid inclusion analyses and SEM observations of the calcite cements, however, did not display any evidence of hydrocarbon generation.

The comparison of the trapping temperatures inferred from microthermometry and clumped isotope thermometry gives coherent results. This suggests that cementation occurred at about 1 km paleoburial depth, as petrographically attested by the crosscutting relationship with compaction stylolites observed in Group I and III veins. The preferential circulation of fluids along reactivated faults was evidenced in chalk. A preexisting fault was reactivated, resulting in vein cementation in the damage zone of the basement fault and the polygonal fault system connected to it. Knowing that paleosealed breccia may cement fault zones in the subsurface is important to predict fault permeability and to identify potential drilling hazards in tight chalk.

6. Conclusion

A petrographical, geochemical, and microthermometric analysis of the calcite veins in the chalk of Flamborough Head (UK) was performed. The geochemical nature of the fluid and the relative timing of fault-controlled fluid flow have been constrained. These new data provide keys to understand the behavior of overpressured fluid flow in fractured tight chalks. The main conclusions are as follows:

- (i) Mineralizing fluids are dominantly meteoric in origin. Fluid flow was probably triggered by Late Cretaceous-Cenozoic tectonic inversion and fluids circulated upward along the damage zone of the major fault.
- (ii) Strontium isotopes demonstrate that mineralizing fluids probably originated from a sandstone aquifer (possibly the Triassic Sherwood Sandstone based on the local stratigraphy).
- (iii) Fluid salinity locally increased through halite dissolution or fluid mixing with connate waters due to the interaction with lithologies overlying the aquifer.
- (iv) In tight chalk, reactivated polygonal fault system was used as preferential fluid flow pathway at different stages of the geological history.
- (v) Estimated crystallization temperatures obtained from both microthermometry and clumped isotopes range between 50 and 65°C.

Disclosure

An earlier version of this work was presented at “International Meeting of Sedimentology,” 2017.

Conflicts of Interest

The authors declare that they have no conflicts of interest.

Acknowledgments

This study has been funded by TOTAL SA, as part of the “Fractured Tight Chalk” project, including the Ph.D. of

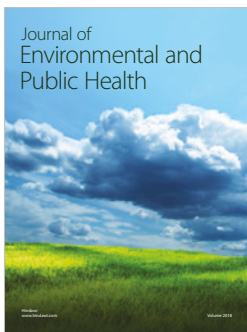
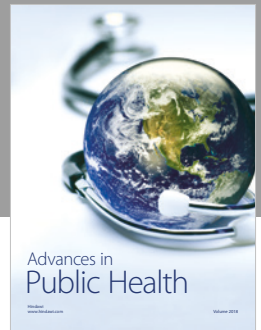
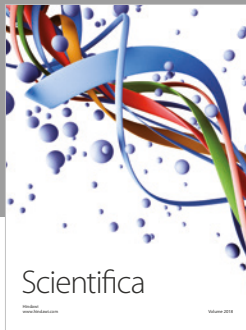
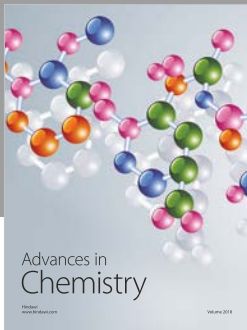
Ophélie Faÿ-Gomord. Thanks are due to Nadine Mattielli from Université Libre de Bruxelles (ULB) for the strontium isotope analyses. The authors also kindly thank Herman Nijs (KU Leuven) for the preparation of the thin sections and wafers, as well as Elvira Vassilieva (KU Leuven) for her contribution to the ICP-OES analyses.

References

- [1] A. J. Mallon, R. E. Swarbrick, and T. J. Katsube, “Permeability of fine-grained rocks: New evidence from chalks,” *Geology*, vol. 33, no. 1, pp. 21–24, 2005.
- [2] P. A. Scholle, “Chalk diagenesis and its relation to petroleum exploration: oil from chalks, a modern miracle?” *AAPG Bulletin (American Association of Petroleum Geologists)*, vol. 61, no. 7, pp. 982–1009, 1977.
- [3] P. Frykman, “Spatial variability in petrophysical properties in Upper Maastrichtian chalk outcrops at Stevns Klint, Denmark,” *Marine and Petroleum Geology*, vol. 18, no. 10, pp. 1041–1062, 2001.
- [4] A. Aydin, “Fractures, faults, and hydrocarbon entrapment, migration and flow,” *Marine and Petroleum Geology*, vol. 17, no. 7, pp. 797–814, 2000.
- [5] P. Paul, M. Zoback, and P. Hennings, “Fluid flow in a fractured reservoir using a geomechanically constrained fault-zone-damage model for reservoir simulation,” *SPE Reservoir Evaluation and Engineering*, vol. 12, no. 4, pp. 562–575, 2009.
- [6] M. Johri, M. D. Zoback, and P. Hennings, “A scaling law to characterize fault-damage zones at reservoir depths,” *AAPG Bulletin*, vol. 98, no. 10, pp. 2057–2079, 2014.
- [7] O. Faÿ-Gomord, C. Allanic, M. Verbiest, E. Lasseur, R. Swennen, and B. Gauthier, “Synsedimentary Polygonal Faults System in Tight Chalk - Multiscale Evidence from Outcrop, Flamborough Head (UK),” in *Proceedings of the 79th EAGE Conference and Exhibition '17*, pp. 4163–4168, Paris, France, June 2017.
- [8] C. Childs, A. Nicol, J. J. Walsh, and J. Watterson, “Growth of vertically segmented normal faults,” *Journal of Structural Geology*, vol. 18, no. 12, pp. 1389–1397, 1996.
- [9] D. C. P. Peacock and D. J. Sanderson, “Strain and scaling of faults in the chalk at Flamborough Head, U.K.,” *Journal of Structural Geology*, vol. 16, no. 1, pp. 97–107, 1994.
- [10] F. G. Bell, M. G. Culshaw, and J. C. Cripps, “A review of selected engineering geological characteristics of English Chalk,” *Engineering Geology*, vol. 54, no. 3–4, pp. 237–269, 1999.
- [11] M. G. Patsoules and J. C. Cripps, “Survey of macro and micro faulting in Yorkshire chalk,” in *Proceedings of the International Chalk Symposium*, pp. 87–93, Thomas Telford, Brighton, London.
- [12] BGS., “The Hydrocarbon prospectivity of Britain’s Onshore Basins,” *Department of Energy and Climate Change (DECC) DEEC*, 83 pages, 2013, https://www.ogauthority.co.uk/media/1695/pages_uk_onshore_2013.pdf.
- [13] I. C. Starmer, “Deformation of the Upper Cretaceous Chalk at Selwicks Bay, Flamborough Head, Yorkshire: its significance in the structural evolution of north-east England and the North Sea Basin,” *Proceedings - Yorkshire Geological Society*, vol. 50, no. 3, pp. 213–228, 1995.
- [14] D. A. Sagi, N. De Paola, K. J. W. McCaffrey, and R. E. Holdsworth, “Fault and fracture patterns in low porosity chalk and their potential influence on sub-surface fluid flow—A case

- study from Flamborough Head, UK,” *Tectonophysics*, vol. 690, pp. 35–51, 2016.
- [15] R. Swennen, H. Ferket, L. Benchilla, F. Roure, and R. Ellam, “Fluid flow and diagenesis in carbonate dominated Foreland Fold and Thrust Belts: Petrographic inferences from field studies of late-diagenetic fabrics from Albania, Belgium, Canada, Mexico and Pakistan,” *Journal of Geochemical Exploration*, vol. 78–79, pp. 481–485, 2003.
- [16] A. Travé, E. Roca, E. Playà, D. Parcerisa, D. Gómez-Gras, and J. D. Martín-Martín, “Migration of Mn-rich fluids through normal faults and fine-grained terrigenous sediments during early development of the Neogene Vallès-Penedès half-graben (NE Spain),” *Geofluids*, vol. 9, no. 4, pp. 303–320, 2009.
- [17] R. H. Sibson, “Fluid involvement in normal faulting,” *Journal of Geodynamics*, vol. 29, no. 3–5, pp. 469–499, 2000.
- [18] J. Richard, M. Coulon, P. Gaviglio, and K. Ramseyer, “L’hydrofracturation: une déformation tectonique à haut potentiel diagénétique. Exemple des craies hydrofracturées de la région d’Omev (Bassin de Paris, France),” *Comptes Rendus de l’Académie des Sciences - Series IIA - Earth and Planetary Science*, vol. 325, no. 5, pp. 359–366, 1997.
- [19] G. A. Kirby and P. W. Swallow, “Tectonism and sedimentation in the Flamborough Head region of north-east England,” *Proceedings - Yorkshire Geological Society*, vol. 46, no. 4, pp. 301–309, 1987.
- [20] T. R. W. Hawkins and R. J. Aldrick, “The pattern of faulting across the western sector of the Market Weighton Block,” in *Proceedings of the Yorkshire Geological and Polytechnic Society*, vol. 50, pp. 125–128, Vale of York, 1994.
- [21] J. Milsom and P. F. Rawson, “The Peak Trough—a major control on the geology of the North Yorkshire coast,” *Geological Magazine*, vol. 126, no. 6, pp. 699–705, 1989.
- [22] R. Tiley, N. White, and S. Al-Kindi, “Linking Paleogene denudation and magmatic underplating beneath the British Isles,” *Geological Magazine*, vol. 141, no. 3, pp. 345–351, 2004.
- [23] A. Emery, “Palaeopressure reconstruction to explain observed natural hydraulic fractures in the Cleveland Basin,” *Marine and Petroleum Geology*, vol. 77, pp. 535–552, 2016.
- [24] K. W. Glennie and P. L. E. Boegner, “Sole Pit Inversion tectonics,” in *Petroleum geology of North-West Europe*, L. V. Illing and G. D. Hobson, Eds., pp. 110–120, 1981.
- [25] J. R. V. Brooks, S. J. Stoker, and T. D. J. Cameron, “Hydrocarbon exploration opportunities in the 21st Century in the UK,” in *Petroleum provinces of the Twenty-first Century*, A. W. Downey, J. C. Threet, and W. A. Morgan, Eds., vol. 74, pp. 167–200, American Association of Petroleum Geologists Memoir, 2001.
- [26] P. F. V. Williams, “Petroleum geochemistry of the Kimmeridge Clay of onshore Southern and Eastern England,” *Marine and Petroleum Geology*, vol. 3, no. 4, pp. 258–281, 1986.
- [27] R. J. Menpes and R. R. Hillis, “Determining apparent exhumation from Chalk outcrop samples, Cleveland Basin/East Midlands Shelf,” *Geological Magazine*, vol. 133, no. 6, pp. 751–762, 1996.
- [28] S. A. Stewart and H. W. Bailey, “The Flamborough Tertiary outlier, UK southern North Sea,” *Journal of the Geological Society*, vol. 153, no. 1, pp. 163–173, 1996.
- [29] I. C. Starmer, “Folding and faulting in the chalk at dykes end, Bridlington Bay, East Yorkshire, resulting from reactivations of the flamborough head fault zone,” *Proceedings of the Yorkshire Geological Society*, vol. 59, no. 3, pp. 195–201, 2013.
- [30] C. Snoeck, J. Lee-Thorp, R. Schulting, J. De Jong, W. Deboege, and N. Mattioli, “Calcined bone provides a reliable substrate for strontium isotope ratios as shown by an enrichment experiment,” *Rapid Communications in Mass Spectrometry*, vol. 29, no. 1, pp. 107–114, 2014.
- [31] D. Weis, B. Kieffer, C. Maerschalk et al., “High-precision isotopic characterization of USGS reference materials by TIMS and MC-ICP-MS,” *Geochemistry, Geophysics, Geosystems*, vol. 7, no. 8, Article ID Q08006, 2006.
- [32] R. H. Goldstein and T. J. Reynolds, *Systematics of Fluid Inclusions in Diagenetic Minerals*, vol. 31, Society for Sedimentary Geology Short Course Series, 1994.
- [33] V. Hurai, M. Huraiová, M. Slobodník, and R. Thomas, *Geofluids: developments in microthermometry, spectroscopy, thermodynamics, and stable isotopes*, Elsevier, London, UK, 2015.
- [34] P. Muchez, J. D. Marshall, J. L. R. Touret, and W. A. Viaene, *Origin and migration of palaeofluids in the Upper Visean of the Campine Basin, northern Belgium*, vol. 41, Sedimentology, Belgium, 1994.
- [35] R. H. Goldstein, E. K. Franseen, and M. S. Mills, “Diagenesis associated with subaerial exposure of Miocene strata, southeastern Spain: Implications for sea-level change and preservation of low-temperature fluid inclusions in calcite cement,” *Geochimica et Cosmochimica Acta*, vol. 54, no. 3, pp. 699–704, 1990.
- [36] E. Roedder, “Metastable superheated ice in liquid-water inclusions under high negative pressure,” *Science*, vol. 155, no. 3768, pp. 1413–1417, 1967.
- [37] F. M. Haynes, “Determination of fluid inclusion compositions by sequential freezing,” *Economic Geology*, vol. 80, no. 5, pp. 1436–1439, 1985.
- [38] R. J. Bodnar, “Revised equation and table for determining the freezing point depression of H₂O-NaCl solutions,” *Geochimica et Cosmochimica Acta*, vol. 57, no. 3, pp. 683–684, 1993.
- [39] Y.-G. Zhang and J. D. Frantz, “Determination of the homogenization temperatures and densities of supercritical fluids in the system NaClKClCaCl₂H₂O using synthetic fluid inclusions,” *Chemical Geology*, vol. 64, no. 3–4, pp. 335–350, 1987.
- [40] M. Bonifacie, D. Calmels, J. M. Eiler et al., “Calibration of the dolomite clumped isotope thermometer from 25 to 350°C, and implications for a universal calibration for all (Ca, Mg, Fe)CO₃ carbonates,” *Geochimica et Cosmochimica Acta*, vol. 200, pp. 255–279, 2017.
- [41] K. J. Dennis, H. P. Affek, B. H. Passey, D. P. Schrag, and J. M. Eiler, “Defining an absolute reference frame for ‘clumped’ isotope studies of CO₂,” *Geochimica et Cosmochimica Acta*, vol. 75, no. 22, pp. 7117–7131, 2011.
- [42] W. F. Defliese, M. T. Hren, and K. C. Lohmann, “Compositional and temperature effects of phosphoric acid fractionation on δ^{47} analysis and implications for discrepant calibrations,” *Chemical Geology*, vol. 396, pp. 51–60, 2015.
- [43] A. Katz, M. Bonifacie, M. Hermoso, P. Cartigny, and D. Calmels, “Laboratory-grown coccoliths exhibit no vital effect in clumped isotope (Δ^{47}) composition on a range of geologically relevant temperatures,” *Geochimica et Cosmochimica Acta*, vol. 208, pp. 335–353, 2017.
- [44] J. Santrock, S. A. Studley, and J. M. Hayes, “Isotopic Analyses Based on the Mass Spectra of Carbon Dioxide,” *Analytical Chemistry*, vol. 57, no. 7, pp. 1444–1448, 1985.
- [45] S.-T. Kim and J. R. O’Neil, “Equilibrium and nonequilibrium oxygen isotope effects in synthetic carbonates,” *Geochimica et Cosmochimica Acta*, vol. 61, no. 16, pp. 3461–3475, 1997.

- [46] S. Mearon, A. Paytan, and T. J. Bralower, "Cretaceous strontium isotope stratigraphy using marine barite," *Geology*, vol. 31, no. 1, pp. 15–18, 2003.
- [47] J. J. Wilkinson, "Metastable freezing: A new method for the estimation of salinity in aqueous fluid inclusions," *Economic Geology*, vol. 112, no. 1, pp. 185–193, 2017.
- [48] I. L. Fabricius and M. K. Borre, "Stylolites, porosity, depositional texture, and silicates in chalk facies sediments. Ontong Java Plateau - Gorm and Tyra fields, North Sea," *Sedimentology*, vol. 54, no. 1, pp. 183–205, 2007.
- [49] J. B. W. Day, "The Occurrence of Groundwater in the United Kingdom," in *Groundwater: Occurrence, Development and Protection*, T. W. Brandon, Ed., p. 615, Institution of Water Engineers and Scientists, London, UK, 1986.
- [50] R. A. Monkhouse and H. J. Richards, "Groundwater resources of the United Kingdom," in *Commission of the European Communities*, Th. Schäfer Druckerei GmbH, Hannover, 1982.
- [51] D. J. Allen, L. J. Brewerton, L. M. Coleby et al., "The physical properties of major aquifers in England and Wales," British Geological Survey Technical Report WD/97/34, Environment Agency R&D Publication, 1997.
- [52] S. D. Burley, "Distribution and origin of authigenic minerals in the Triassic Sherwood Sandstone Group, UK," *Clay Mineralogy*, vol. 19, no. 3, pp. 403–440, 1984.
- [53] R. H. Worden, D. A. C. Manning, and S. H. Bottrell, "Multiple generations of high salinity formation water in the Triassic Sherwood Sandstone: Wytch Farm oilfield, onshore UK," *Applied Geochemistry*, vol. 21, no. 3, pp. 455–475, 2006.
- [54] S. Schmid, R. H. Worden, and Q. J. Fisher, "Diagenesis and reservoir quality of the Sherwood Sandstone (Triassic), Corrib Field, Slyne Basin, west of Ireland," *Marine and Petroleum Geology*, vol. 21, no. 3, pp. 299–315, 2004.
- [55] R. N. Clayton, I. Friedman, and D. L. Graf, "The origin of saline formation waters: 1. Isotopic composition," *Journal of Geophysical Research: Atmospheres*, vol. 71, no. 16, pp. 3869–3882, 1966.
- [56] G. E. Strong, A. E. Milodowski, J. M. Pearce, S. J. Kemp, S. V. Prior, and A. C. Morton, "The petrology and diagenesis of Permo-Triassic rocks of the Sellafeld area, Cumbria," *Proceedings of the Yorkshire Geological Society*, vol. 50, no. 1, pp. 77–89, 1994.
- [57] P. J. Greenwood and S. M. Habesch, "Diagenesis of the Sherwood Sandstone Group in the southern East Irish Sea Basin (Blocks 110/13, 110/14 and 110/15): Constraints from preliminary isotopic and fluid inclusion studies," *Geological Society, London, Special Publications*, vol. 124, pp. 353–371, 1997.
- [58] G. E. Strong and A. E. Milodowski, "Aspects of the diagenesis of the Sherwood Sandstones of the Wessex Basin and their influence on reservoir characteristics," *Geological Society, London, Special Publications*, vol. 36, pp. 325–337, 1987.
- [59] A. J. C. Hogg, A. W. Mitchell, and S. Young, "Predicting well productivity from grain size analysis and logging while drilling," *Petroleum Geoscience*, vol. 2, no. 1, pp. 1–15, 1996.
- [60] D. B. Kemp, A. L. Coe, A. S. Cohen, and L. Schwark, "Astrophysical pacing of methane release in the Early Jurassic period," *Nature*, vol. 437, no. 7057, pp. 396–399, 2005.
- [61] A. Parker, "The clay mineralogy and some trace element contents of the Speeton clay," *Proceedings of the Yorkshire Geological Society*, vol. 40, no. 2, pp. 181–190, 1974.
- [62] H. Dypvik, "Geochemical compositions and depositional conditions of Upper Jurassic and Lower Cretaceous Yorkshire clays, England," *Geological Magazine*, vol. 121, no. 5, pp. 489–504, 1984.
- [63] R. M. S. Perrin, "The Clay Mineralogy of British Sediments. London," in *Mineralogical Society*, vol. 247, p. 247, London, UK, 1971.
- [64] R. J. Merriman and C. V. Jeans, "In Oil Shale Resources in Great Britain (Gallois, R. W.)," *Appendix C. Institut of Geological Sciences Open File Rpt*, pp. C1–C9, 1979.
- [65] J. R. Boles and S. G. Franks, "Clay diagenesis in Wilcox sandstones of Southwest Texas; implications of smectite diagenesis on sandstone cementation," *Journal of Sedimentary Research*, vol. 49, pp. 55–70, 1979.
- [66] M. Safaricz and I. Davison, "Pressure solution in chalk," *AAPG Bulletin*, vol. 89, no. 3, pp. 383–401, 2005.
- [67] O. Faÿ-Gomord, J. Soete, K. Katika et al., "New insight into the microtexture of chalks from NMR analysis," *Marine and Petroleum Geology*, vol. 75, pp. 252–271, 2016.
- [68] N. J. Shackleton, J. P. Kennett et al., "Paleotemperature history of the Cenozoic and the initiation of Antarctic glaciation: oxygen and carbon isotope analyses in DSDP sites 277 279 and 281," in *Initial reports of the Deep Sea Drilling Project 29*, J. P. Kennett, R. E. Houtz et al., Eds., pp. 743–755, U.S. Government Printing Office, Wash, D.C, USA, 1975.
- [69] A. Zanella, P. R. Cobbold, and T. Boassen, "Natural hydraulic fractures in the Wessex Basin, SW England: Widespread distribution, composition and history," *Marine and Petroleum Geology*, vol. 68, pp. 438–448, 2015.
- [70] J. De Jager, "Geological development," in *Geology of the Netherlands*, T. h. E. Wong, D. A. J. Batjes, and J. De Jager, Eds., pp. 5–26, Royal Netherlands Academy of Arts and Sciences, Amsterdam, 2007.



Hindawi

Submit your manuscripts at
www.hindawi.com

